

# Seismic Performance of Energy-Efficient Structural Insulated Panels

**K.M. Mosalam, M.S. Günay**

*University of California, Berkeley*



## SUMMARY

This paper reports results of an investigation of the seismic performance of structural insulated panels (SIPs). For this purpose, a test program consisting of cyclic and hybrid simulation tests is pursued. Seven SIPs and a conventional wood panel are tested within this context. Evaluated test results include global force-displacement responses and local displacement measurements. In addition, the energy-efficiency of SIPs is demonstrated compared to conventional wood panels from heat transfer analyses. The research findings include similar structural performance of the tested SIPs and conventional wood panels, significant effect of the nail spacing on the response of SIPs, and the benefits of hybrid simulation in evaluating the structural performance. Conducted heat transfer analyses showed superior thermal insulation characteristics of SIPs and the thermal bridging effects introduced by the presence of vertical studs in the conventional wood panels.

*Keywords: Finite element analysis, heat transfer, hybrid simulation, structural insulated panel, wood shear wall.*

## 1. INTRODUCTION

Structural insulated panels (SIPs) represent an example of a structural system mainly employed for energy-efficient construction. They are composed of an energy-efficient core such as expanded polystyrene (EPS) with both traditional and novel facing materials such as plywood, oriented strand board (OSB), cement mortar, or steel, Fig. 1.1. There is considerably few information available about the seismic behavior of SIPs. Developed over 50 years ago, SIPs are extensively used throughout Europe and North America. Their application in seismically hazardous regions is limited due to unacceptable performance as demonstrated by cyclic testing. While there is a growing database of SIPs tests, no research has attempted to subject the panels to realistic dynamic loading regimes. Hybrid simulation (HS) - where various structural configurations can be modelled analytically and accordingly reasonable cost and time savings are realized for testing large number of specimens - comes forward as a suitable and efficient method for testing SIPs under realistic dynamic loading regimes. Within this perspective, seismic performance of SIPs has been investigated by testing seven SIPs and a conventional wood panel using cyclic testing and HS.

## 2. TEST SETUP, TEST MATRIX AND INSTRUMENTATION

The different parts of the test setup and one of the test specimens are shown in Fig. 2.1. The displacements (computed during HS or determined beforehand in cyclic testing) are applied through a loading tube which is prevented from moving out of plane, Fig. 2.1a. Pure shear loading is provided by a scissors mechanism, Fig. 2.1b, attached to the top of the specimen which forces the top side and the support beam side, Fig. 2.1c, to remain parallel. The test setup is designed to allow in-plane testing of 8 ft×8 ft panels and gravity loading of 3 kips applied through a gravity frame in most tests, Fig. 2.1d. The panels consist of two 7/16" OSB skins with a 3-5/8" thick EPS foam core (overall panel thickness of 4-1/2") and two 4 ft×8 ft panels connected with panel-to-panel thermal (box) spline.

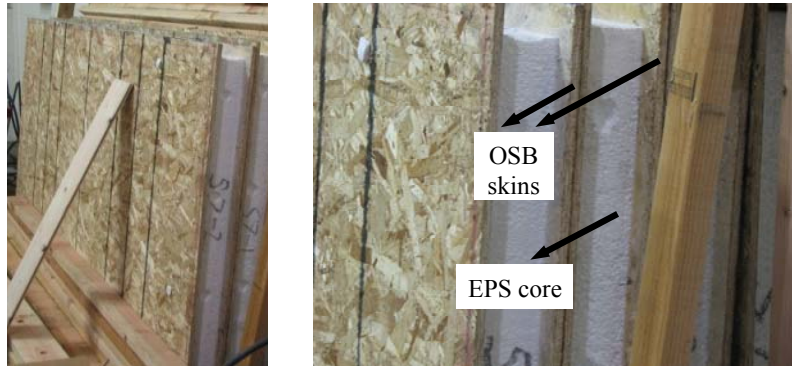


**Figure 1.1** Structural insulated panels with ESP core and OSB skin

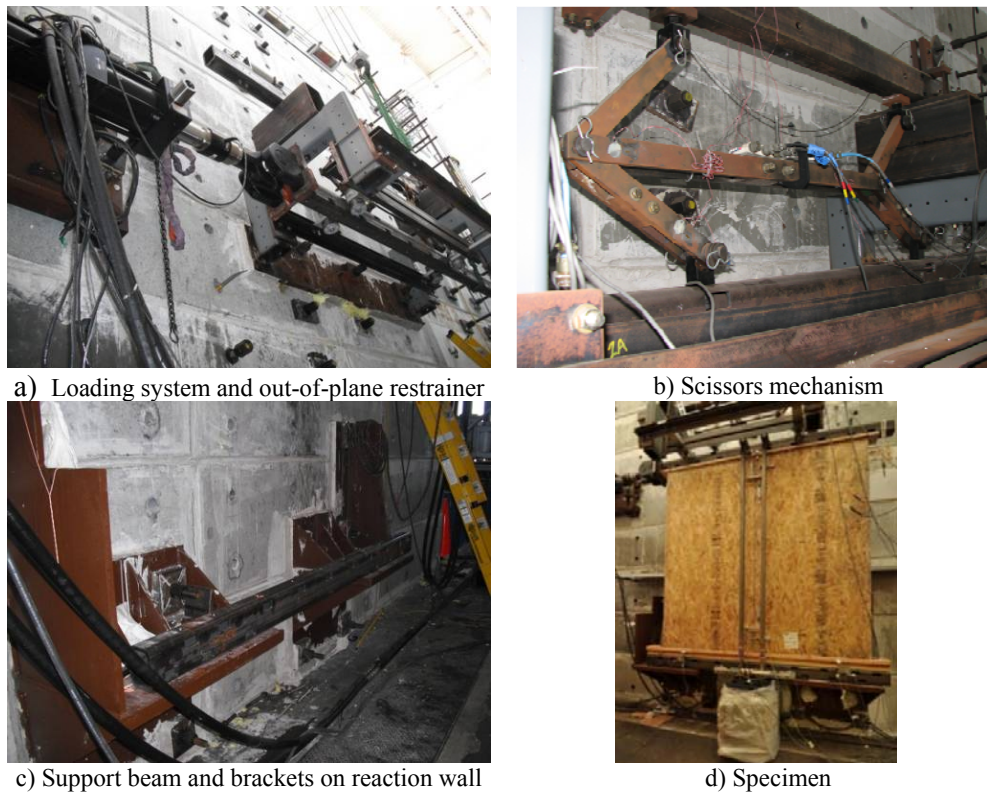


**Figure 2.1** Test setup and test specimen

The test matrix is given in Table 2.1. This matrix allows the comparison of the seismic performance of SIPs with a conventional wood panel and studying effects of various parameters on the response of SIPs. These parameters include: (a) nail spacing, a parameter related to the design and construction of panels, (b) parameters related to loading such as the presence of gravity loading and the effect of lateral loading pattern, CUREE protocol (Krawinkler et al. 2000) vs. HS, (c) type of ground motion (GM), near-fault vs. far-field, and (d) a parameter related to HS, presence of an analytical substructure.

In addition to the load cell and LVDT of the actuator which determine the global response of the specimen, displacement transducers are placed at various locations of the panels to measure the vertical sliding and horizontal opening between the two panels, the uplift at the bottom, and the sliding between the loading tube and the specimen, Fig. 2.2. The vertical sliding and horizontal opening are directly related to the response of the panels. Uplift measurements at the bottom is for the determination of the presence of any rocking at the base, which consists of two 2"×4" and a single

2"×6" untreated Douglas-fir structural grade lumber secured to the support beam with eight fully threaded 5/8" bolts. Fasteners are 8d common bright nails –nails with a normal surface finish. All facing materials are bearing on the top and bottom lumber pieces. End posts are double 2×4 for attaching external hold-down of the type UPS PHD6. Value of the sliding between the loading tube and the specimen is subtracted from the actuator displacement in order to calculate the global specimen displacement. Strain gages are installed on the scissor mechanism and the two front long vertical steel tubes holding the gravity loading.

**Table 2.1** Test matrix

Specimen	Protocol	Gravity	Nail spacing [in]	Remarks
S1	CUREE	No	6	Conventional wood panel
S2	CUREE	No	6	-
S3	CUREE	Yes	6	-
S4	HS	Yes	6	Near-fault pulse-type GM
S5	HS	Yes	3	Near-fault pulse-type GM
S6	CUREE	Yes	3	-
S7	HS	Yes	3	Long duration, harmonic GM
S8	HS	Yes	3	Near-fault GM; 3 stories computational substructure

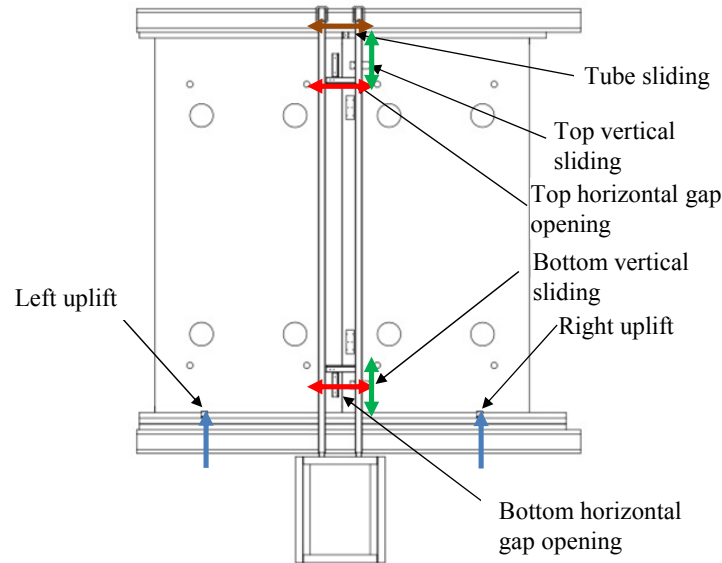


**Figure 2.2** Location of displacement transducers to measure local deformations

### 3. HYBRID SIMULATION DETAILS

HS is a testing method, where the response of a structure under external dynamic excitation, e.g. due to GM, is obtained through numerical integration of the governing equations of motion. The structure is typically idealized into several substructures where some are modeled analytically and the others are physically tested with measured responses used in the computational algorithm to advance the numerical integration. Combining realistic dynamic excitation in shaking table tests, which are expensive and/or restrictive for the specimen sizes, with ability to test large-scale structures in the simpler quasi-static testing, HS came forward as a cost-effective alternative for structural testing. A summary of the literature on various aspects of HS is given in (Mosalam and Günay 2011).

Specimens S4, S5, and S7 are tested with HS where SIPs specimen is modeled as a single degree of freedom (SDOF) system with only analytical mass and damping without the presence of any analytical substructure in these tests. In order to obtain representative period and strength ratio (strength/weight) values, computational mass and damping ratios are chosen as 32.5 slug and 0.05, respectively. HS has

the ability to partition a structure into experimental and analytical substructures, thereby eliminating the need to test the whole structure. Therefore, specimen S8 is tested with HS including an analytical substructure where 3 upper stories are modeled analytically in addition to the physical specimen, Fig. 3.1. Force-displacement relationship of the upper stories (represented by nonlinear springs in Fig. 3.1) is obtained by matching analytically the force-displacement relationship of specimen S5.

Two ground motions with different characteristics are employed in HS. The GM from Los Gatos station of 1989, Loma Prieta earthquake, is a pulse-type near-fault GM. GM from Vinadel Mar station of 1985, Chile earthquake, is a long duration GM with several harmonic cycles, Fig. 3.2. Both ground motions are applied in five intensity levels: 1) Elastic, 2) 0.5 Design Earthquake (0.5DE), 3) Design Earthquake (DE), 4) Maximum Considered Earthquake (MCE), and 5) 1.5 MCE. Elastic level test is conducted to make sure the test setup and instrumentation are properly functioning. Scales for the other intensity levels are based on the spectral acceleration for the considered hazard levels.

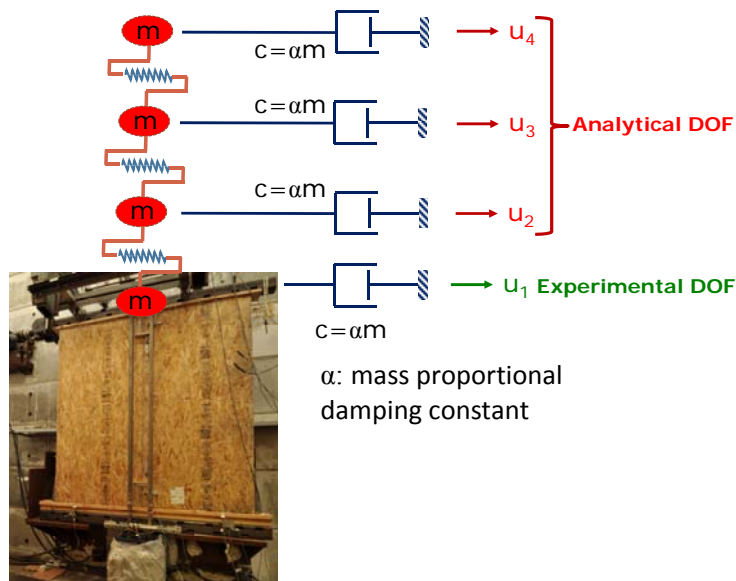


**Figure 3.1** HS of S4, S5, and S7 (without  $u_2$ ,  $u_3$ , and  $u_4$ ) and S8

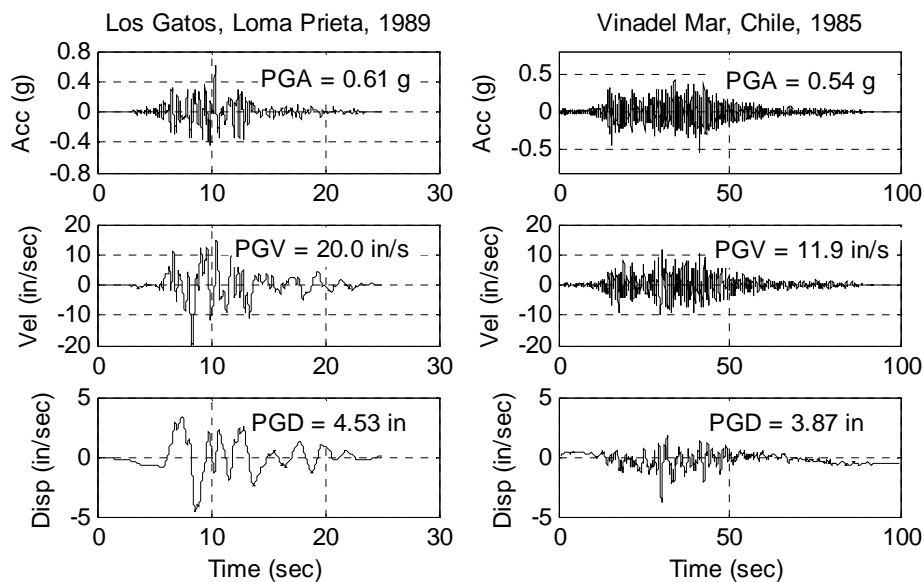


**Figure 3.2** Acceleration, displacement and velocity time histories of the ground motions utilized in HS tests

#### 4. EVALUATION OF TEST RESULTS

The envelope of the full force-displacement history, Fig. 4.1, is employed for the evaluation of global response of the specimens, Fig. 4.2. Some of the parameters derived from the envelope curves are listed in Table 4.1. It should be noted that “Hysteretic Energy” in this table is obtained as the area enclosed by the hysteretic loops using the full force-displacement history. Peak and residual global displacements of the specimens are presented separately in Table 4.2. Finally, peaks of local displacement measurements are summarized in Table 4.3.

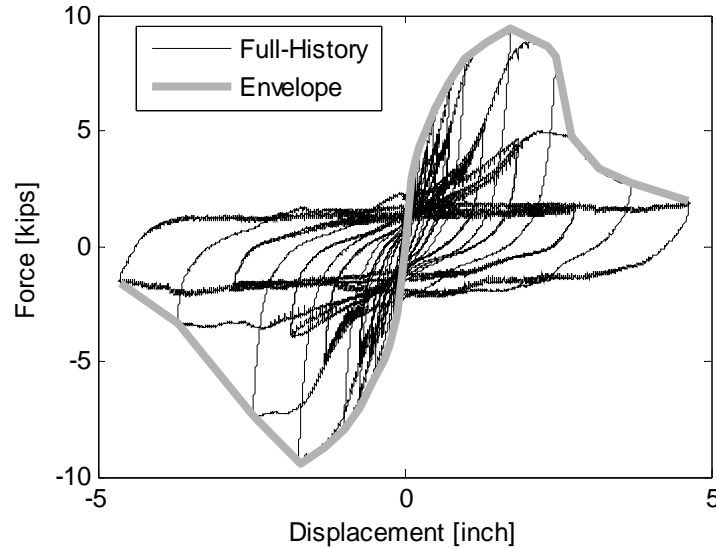


Figure 4.1 Force-displacement history and enclosing envelope for S3

Table 4.1 Global response parameters

Specimen	S1	S2	S3	S4	S5	S6	S7	S8
Initial Stiffness [kip/in]	46.2	12.2	23.4	22.9	35.5	32.7	33.2	38.3
Force Capacity [kip]	12.2	11.4	9.5	8.6	15.6	16.2	15.5	16.0
Ductility <sup>*,†</sup>	7.0	3.6	3.5	2.5	3.7	4.8	3.4	4.0
Hysteretic Energy [kip-in]	201.8	193.1	189.2	152.7	363.1	309.9	1077.8	237.4

\*Displacement at  $0.75 \times$  peak force (square in Fig. 4.2) divided by yield displacement (circle in Fig. 4.2)

†Average of values in positive and negative directions

Table 4.2 Peak and residual global displacements

Specimen	S1,S2 S3,S6	DE				MCE				1.5MCE			
		S4	S5	S7	S8	S4	S5	S7	S8	S4	S5	S7	S8
Peak Disp. (+)	4.7	2.7	1.3	1.1	1.2	4.7	3.5	2.2	2.4	-	5.8	3.3	-
Peak Disp. (-)	-4.7	-2.8	-1.0	-1.0	-1.7	-	-3.2	-2.0	-3.1	-	-	-4.2	-
Residual Disp.	0.0	1.5	0.1	0.0	0.0	-	0.8	0.0	0.4	-	-	0.3	-

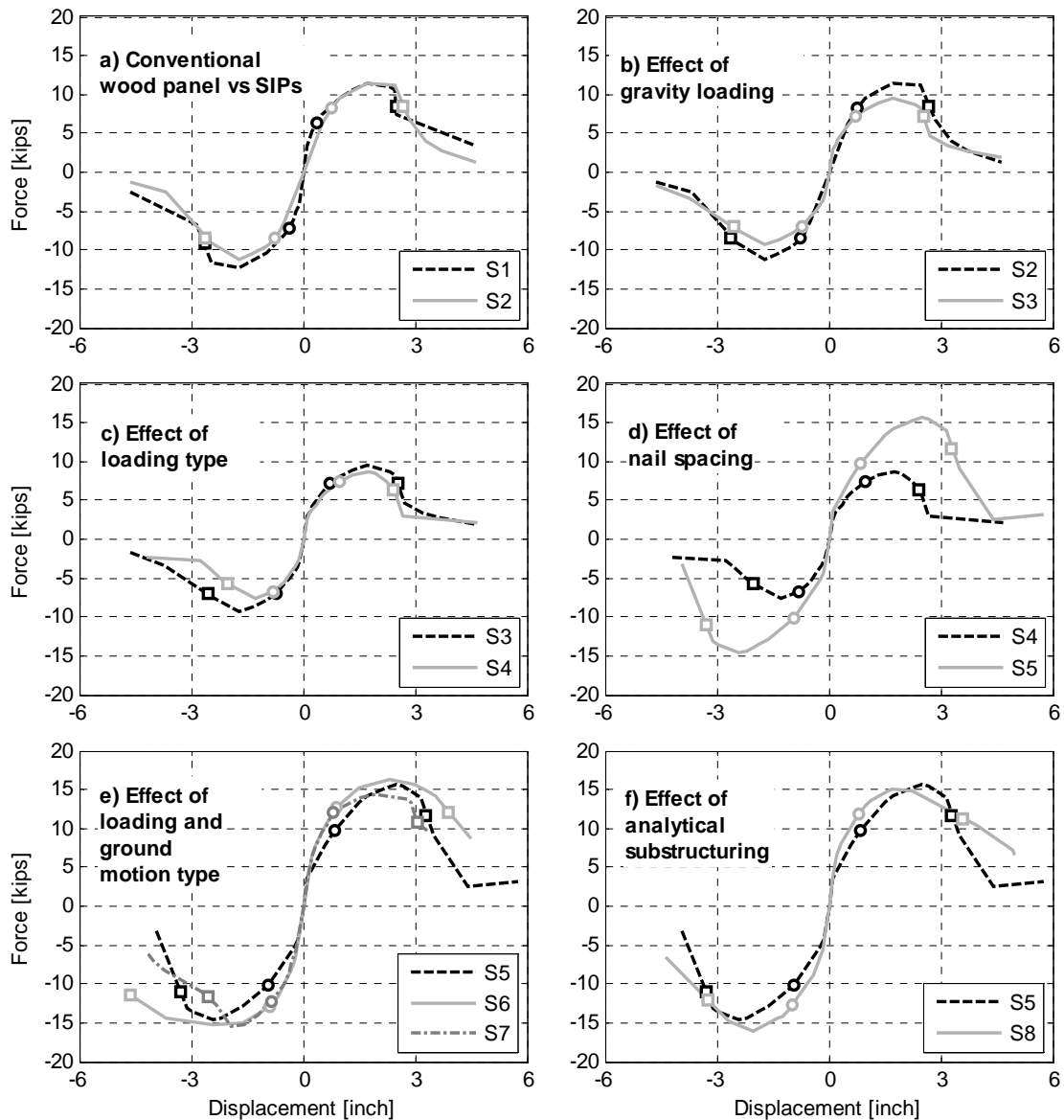


Figure 4.2 Envelope curves of test specimens

#### 4.1 Comparison of Conventional Wood Panel and SIPs (S1 vs S2)

Conventional wood panel (S1) and SIPs (S2) specimens have similar force-displacement envelopes, Fig. 4.2a, with S1 having slightly larger force capacity. Main differences between the specimens are the initial stiffness and ductility values. Ratio of the stiffness and ductility of S1 to those of S2 are almost 4 and 2, respectively. Initial stiffness difference is due to different vertical stud spacing, i.e. 96" in S2 vs. 16" in S1. It is noted that same thickness OSB skins are provided in both sides for S1 and S2. Similar to the case of stiffness, one would expect the force capacity of S1 to be much higher than that of S2. However, force capacities of both specimens are similar which is explained by observed damage of S1, where most of the damage was nail pull out in the fasteners along the seam between the two panels and the connections at the top and bottom. Such damage limited full use of all vertical studs and accordingly limited the force capacity to that dictated by the fasteners. Although structural performance of S1 can be viewed as superior compared to S2 considering ductility, this performance difference is not large enough to overcome the benefit of significant energy efficiency offered by S2.

In order to compare the energy-efficiency of S1 and S2, heat transfer analyses are conducted with the finite element method using THERM 6.3 (2011), software developed at Lawrence Berkeley National Laboratory for modeling and analyzing heat-transfer effects in building components. For this purpose, sections of S1 and S2 are modeled with the correct geometry, materials, and thermal boundary conditions, Fig. 4.3. Analysis results show that the studs form thermal bridges where heat flux abruptly increases. In addition to heat flux contours, R-factor [hr-ft<sup>2</sup>-°F/Btu], a measure of the thermal conductivity, is reported in Fig. 4.3. R-factor is calculated as the temperature difference between two boundaries multiplied by the distance between the boundaries and divided by the integrated heat flux between the boundaries. Therefore, as R-factor increases, energy-efficiency increases. Thermal insulation efficiency of SIPs is confirmed by R-factor which is 3.5 times large for S2 compared to S1.

**Table 4.3** Peaks of local displacements [in]

Specimen	Bottom ver. disp.	Bottom hor. disp.	Top ver. disp.	Top hor. disp.	Uplift right	Uplift left	Tube sliding
S2	0.71	0.04	0.73	0.27	0.02	0.02	0.02
S3	0.49	0.01	0.50	0.14	0.03	0.02	0.03
S6	1.23	0.15	1.08	0.13	0.14	0.18	0.18
DE	S4	0.39	0.01	0.37	0.09	0.07	0.00
	S5	0.26	0.02	0.27	0.03	0.08	0.18
	S7	0.23	0.02	0.21	0.02	0.15	0.02
	S8	0.37	0.03	0.37	0.04	0.09	0.11
MCE	S4	0.15	0.01	0.16	0.02	0.03	0.01
	S5	0.63	0.05	0.64	0.09	0.14	0.19
	S7	0.45	0.03	0.43	0.04	0.53	0.06
	S8	0.65	0.03	0.55	0.05	0.16	0.27
1.5 MCE	S4	-	-	-	-	-	-
	S5	0.51	0.05	0.52	0.06	0.06	0.09
	S7	0.55	0.08	0.54	0.06	0.59	0.06
	S8	-	-	-	-	-	-

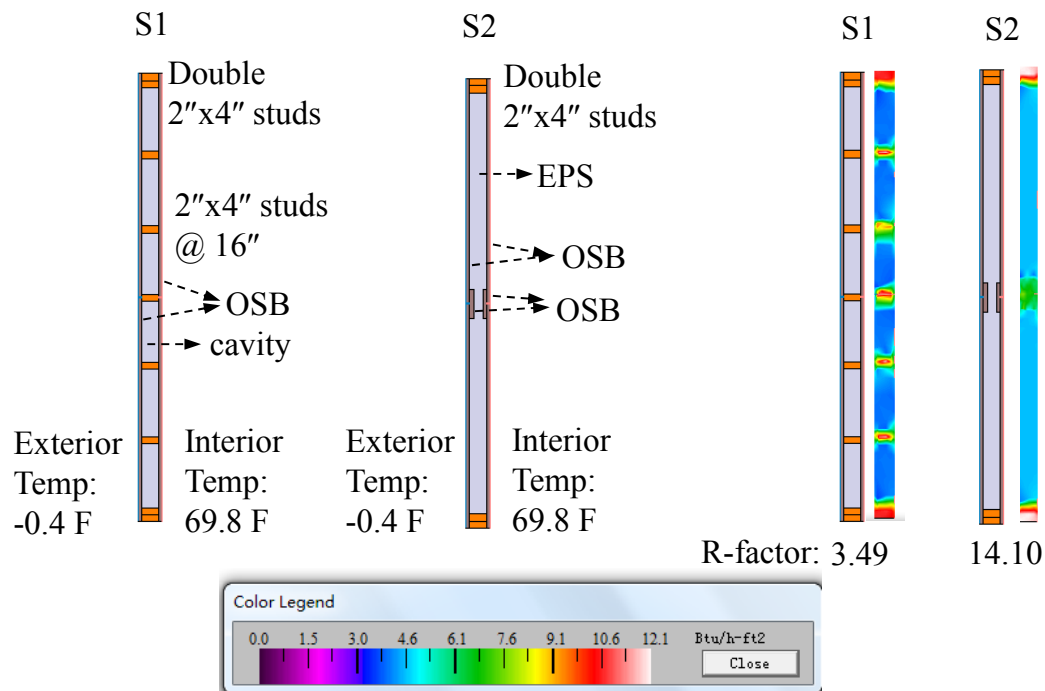


**Figure 4.3** Heat transfer analysis of S1 and S2

#### **4.2 Effect of Gravity Loading on SIPs (S2 vs S3)**

The specimen with 3 kips gravity loading (S3) possesses greater initial stiffness and smaller force capacity compared to that without gravity loading (S2), whereas the ductility and hysteretic energy values are similar, Fig. 4.2b. It should be noted that the gravity loading does not introduce additional lateral forces since the steel tubes holding the gravity load are kept vertical during testing due to low velocity. This is verified by negligible strains on these steel tubes. It is observed that the gravity loading reduces the vertical sliding and gap opening between the panels, especially the 0.27" peak sliding at the top of S2, which is greater than the peaks measured in other specimens, is reduced to half. Since the test with gravity loading represents a more realistic condition and results in differences in the specimen behavior compared to the no gravity case, S3 to S8 are tested with gravity loading.

#### **4.3 Effect of Loading Type on SIPs (S3 vs S4 & S6 vs S5 & S7)**

Envelope curves of S3 and S6 tested with cyclic loading cover a slightly broader area than the envelope curves of the corresponding specimens S4 and S5 & S7 tested with HS, Fig. 4.2c and Fig. 4.2e. Maximum vertical sliding of S6 is almost twice those of S5 and S7. Similar observation is valid for comparison of S3 and S4 but to a lesser extent. Accordingly, CUREE protocol for ordinary ground motions is more critical for local deformations compared to HS with ordinary or near-fault GMs.

HS allows investigating the case-specific effect of different ground motions in terms of asymmetric displacement cycles and residual displacements, Table 4.2. For example, S4 has a significant residual displacement of 1.5" (1.5% drift) at the end of DE level, consistent with last cycles of the CUREE protocol for near-fault ground motions, which have an origin defined by a residual offset displacement (Krawinkler et al. 2000). However, this offset displacement is a constant fraction of the maximum displacement, whereas this fraction is actually not constant for different specimens even excited by the same GM as for S4 and S5. Moreover, S7 results in asymmetric peak displacements of 3.3" and -4.2" different from the symmetric displacements of the CUREE protocol for ordinary ground motions.

#### **4.4 Effect of Nail Spacing on SIPs (S4 vs S5 & S3 vs S6)**

Nail spacing has a significant influence on the force-displacement response of SIPs, Fig. 4.2d. Initial stiffness, force capacity and hysteretic energy of S5 and S6 with 3" nail spacing are significantly larger than those of S4 and S3 with 6" nail spacing. The increase of force capacity is attributed to attainment of full capacity of vertical studs as a result of decreased nail spacing. However, increase of initial stiffness indicates that contribution of the panels to the structural performance also increases because of decreased nail spacing. Moreover, ductility of S5 and S6 are greater than that of S4 and S3.

It is noted that the peak vertical sliding of S6 is almost 2.5 times that of S3. Since S6 is subjected to larger lateral force, peak vertical shear force between the two panels is larger for S6 leading to greater vertical sliding. Similar observation is valid for the comparison of S4 and S5 but to a lesser extent. Maximum force takes place at DE intensity level for S4 where the maximum vertical sliding is 0.39" whereas it occurs at MCE intensity level for S5 where the maximum sliding is 0.63". It is noted that the displacement limit of the stroke of the actuator is reached in MCE and 1.5 MCE levels for S4 and S5, respectively, indicating that the specimen with smaller nail spacing can survive higher earthquake intensities. Moreover, residual displacement at end of DE level of S5 is much smaller than that of S4, even residual displacement at end of MCE level of S5 is about half that of S4 at end of DE level.

#### **4.5 Effect of GM Type on SIPs (S5 vs S7)**

Initial stiffness, force capacity and ductility of specimens tested with the pulse-type GM (S5) and long duration harmonic GM (S7) are very similar, Fig. 4.2 e. However, hysteretic energy dissipated by S7 is almost three times that dissipated by S5 due to the longer duration and greater number of cycles. Actuator displacement limit of 5.8" is reached at 1.5 MCE level during testing S5. However, peak

displacement is only 4.1" at 1.5 MCE level for S7. Similarly, residual displacement of S5 (0.7") is much larger than that of S7 (0.1") at MCE level. In addition, peak vertical sliding (average of top and bottom sliding) of S5 (0.64") is also larger than that of S7 (0.44") at MCE level. It is noted that horizontal gap opening is small at all intensity levels for all specimens. Based on global and local displacements, it is concluded that a near-fault pulse-type GM is more critical and damaging for SIPs compared to a long duration GM with many cycles.

#### **4.6 Effect of Analytical Substructuring on SIPs (S5 vs S8)**

Initial stiffness, force capacity and ductility of S8 and S5 tested with HS with and without analytical substructuring using pulse-type GM are similar, fig. 4.2f. However, slope of the force-displacement relationship after the initial linear part is larger for S8 due to variability in the construction of the specimens and leads to smaller peak and residual displacements of S8 at MCE level. The differences in the structural configuration (i.e. a single story vs four story structure) contribute to the differences in the response. However, the amount of this contribution is unknown because of the different force-displacement characteristics of the specimens. As opposed to the global response, peak local displacements of S5 and S8 are similar.

### **5. CONCLUDING REMARKS**

Conclusions of the conducted investigation are as follows:

- Tested conventional wood panel and SIPs produced similar force-displacement envelopes. Although structural performance of the conventional wood panel is somewhat superior compared to the SIPs considering ductility and initial stiffness, this performance difference is not large enough to overcome the benefit of the significant energy efficiency offered by SIPs.
- A finite element heat transfer analyses show the thermal insulation efficiency of SIPs compared to conventional wood panels and the thermal bridging introduced by vertical studs.
- Existence of gravity loading leads to greater initial stiffness and smaller force capacity and reduces the vertical sliding and gap opening between the SIPs.
- Effect of nail spacing is significant on the structural performance of SIPs. The global force-displacement response is significantly improved by the reduction of nail spacing. However, increase in the force capacity due to reduced nail spacing results in larger vertical shear forces which in turn increases the amount of vertical sliding.
- CUREE protocol for ordinary ground motions is too conservative for local deformations compared to HS with ordinary and even near-fault ground motions.
- HS allows investigation of the case-specific effect of different ground motions in terms of asymmetric displacement cycles and residual displacements.
- Based on the global and local displacements, near-fault pulse-type GM is more critical and damaging for SIPs compared to long duration GM with many cycles.
- Based on the similar responses of SIPs and conventional wood frame panels, the above three conclusions are likely to be valid for the conventional wood panels.
- Global responses of SIPs with and without analytical substructuring are somewhat different due to different structural configurations and force-displacement properties demonstrating the need for analytical substructuring as a part of the performance evaluation.

### **ACKNOWLEDGEMENTS**

The authors acknowledge the financial support under the Intra-University Transaction No. 6815031 from the LBNL under Contract No. DE-AC02-05CH11231 of the US-DOE. The technical support of Dr. Richard C. Diamond is greatly appreciated. The support of nees@berkeley staff and students was essential to the experimental research. The SIPs were donated with help of Mr. Bill Wachtler, SIPA, and Mr. Jim Whalen, PFB Corporation.

## REFERENCES

- Krawinkler, H., Parisi, F., Ibarra, L., Ayoub, A., and Medina, R. (2000). Development of a testing protocol for wood frame structures, *CUREE Publication*, No. W-02, California.
- Mosalam, K.M. and Günay, S. (2011). Overview of hybrid simulation framework with application examples, *Proceedings of a Workshop in Honor of Prof. P. Gülkan*, Middle East Technical University, Ankara, Turkey, October, 14.
- Mosalam, K.M. and Mahin, S.A. (2007). Seismic evaluation and retrofit of asymmetric multi-story wood-frame building, *Journal of Earthquake Engineering*, 11(6): 968-986.
- THERM 6.3. (2011). <http://windows.lbl.gov/software/therm/therm.html>.